Spectral-brightness pyrometry: Radiometric measurements of non-uniform temperature distributions

CrossMark

I.P. Gulyaev [a,b,*], A.V. Dolmatov [b]

[a] Khristianovich Institute of Theoretical and Applied Mechanics SB RAS, Institutskaya Str. 4/1, Novosibirsk 630090, Russia
[b] Ugra State University, Chekhova Str. 16, Khanty-Mansiysk 628012, Russia

ABSTRACT

The paper proposes spectral-brightness pyrometry (SBP) as a new approach to measure the temperature field dynamics on the emitting body surface. The brief review of modern methods of pyrometry – radiometric temperature measurements – is presented. Their properties are analyzed in the Wien's approximation. The SBP combines the high resolution on temperature, time, and space typical for the brightness pyrometry instruments, and small methodical error of temperature measurements of materials with unknown emissivity intrinsic for spectral pyrometers. The peculiarity of this method is calibration of the brightness pyrometer – thermal vision camera – directly during the measurement process using the integral thermal radiation spectrum of the object. The mathematical model of the SBP measurement system is proposed, the technique of data processing based on this model is verified. The examples of practical implementation of the SBP method for the determination of temperature field dynamics of objects with unknown emissivity are presented.

© 2017 Elsevier Ltd. All rights reserved.

1. Introduction

It would be hard to overestimate the importance of temperature measurements based on the spectrum of objects thermal radiation. These tasks are solved both in advanced sciences, from astrophysics to micro- and nano-world studies, and in everyday industrial practice. Despite such a wide range of problems, the differences of them are pure quantitative, i.e. the order of measured temperatures, operational region of electromagnetic radiation spectrum, the type of utilized photo-detectors. The pyrometric methods offer the advantages of non-contact measurements with minimal influence on the investigated object, high spatial and temporal resolution of control instruments, and wide range of measurable temperatures.

It can be argued that the methodology of most optical pyrometry types used today was developed about a hundred years ago [1] and since then there have been few fundamental changes in its scientific base. In general, the development of optical temperature measuring instruments followed the emergence of new photo-detecting elements (photomultipliers, photodiodes, CMOS and CCD arrays, etc.) and digital acquisition systems. The first brightest

pyrometers of the early 1900s [2], based on the principle of a "disappearing filament", as well as later instruments measuring the absolute brightness of thermal radiation at a certain wavelength, were extremely widespread due to simplicity and high sensitivity, but they had a significant drawback - the measured "brightness" temperature of the surface with low emissivity significantly differs from its true temperature. The appearance of multi-wave and spectral photo-detecting devices in the middle of the 20th century has made it possible to increase the accuracy of measurements, to control the presence of a non-thermal signal component, even to make estimates of the material emissivity spectral dependence. However, in fact, the method of measuring the temperature, including the utilization of Wien's auxiliary coordinates, was borrowed from a well-developed approach of two-color pyrometry [3].

The aim of present work is to introduce a new approach of spectral-brightness pyrometry, which combines the best qualities of known methods of radiometric temperature measurements. For this purpose, we present a systematic overview of the main pyrometric methods, in which we consider their strengths and weaknesses.

2. Thermal radiation

All the pyrometric methods are based on the law of thermal radiation. Bodies emit light as a result of atoms and molecules

* Corresponding author at: Khristianovich Institute of Theoretical and Applied Mechanics SB RAS, Institutskaya Str. 4/1, Novosibirsk 630090, Russia.
E-mail address: gulyaev@itam.nsc.ru (I.P. Gulyaev).

Nomenclature

λ	radiation wavelength	
T	body temperature	
$r(\lambda,T), b(\lambda,T)$	spectral radiance (spectral brightness) of the black body and a real body	
ε	material emissivity	

Constants
$c = 2.998 \cdot 10^8$ m/s speed of light in vacuum,
$h = 6.626 \cdot 10^{-34}$ J·s Plank's constant,
$k = 1.38 \cdot 10^{-23}$ J/K Boltzmann's constant,
$C_1 = 3.7418 \cdot 10^{20}$ W·nm^4·m^{-2} first radiation constant,
$C_2 = 14.388 \cdot 10^6$ nm·K second radiation constant.

---

transition from the states with higher energy into the states with lower energy. Population of high-energy levels can be provided by the equilibrium thermal motion of atoms and molecules which is characterized in terms of body temperature or by the external action, such as radiation, chemical reactions, electric current, etc. In the first case, the body radiation is called thermal, in the second – the luminescence. At the turn of the XIX – XX centuries, Max Plank obtained the law of equilibrium thermal radiation of an absolute black body, using the concept of the discrete energy levels of radiating oscillators and the Boltzmann's theorem of the energy level population. The black body is an idealized object which completely absorbs the incident radiation, and real bodies correspond to it to some extent only. The Plank's law determines the power of electromagnetic radiation into the semi-space from a black body unit area in the unit wavelength range (*spectral brightness*) [4]:

$$r(\lambda,T) = \frac{2\pi hc^2}{\lambda^5} \cdot \frac{1}{\exp(hc/\lambda kT) - 1} \left[\frac{W}{m^2 \cdot m}\right]. \tag{1}$$

In practice, when the wavelength is measured in nanometers, and object area in millimeters, it is convenient to use the values of pyrometric (radiation) constants: $C_1 = 2\pi hc^2 = 3.7418 \cdot 10^{20}$ W·nm^4/m^2, $C_2 = hc/k = 14.388 \cdot 10^6$ nm·K. When the condition $C_2/\lambda T \gg 1$ is satisfied, unity in the denominator can be neglected, and formula (1) takes on the form called the Wien's approximation:

$$r(\lambda,T) = \frac{C_1}{\lambda^5} \cdot \exp(-C_2/\lambda T) \quad \left[\frac{W}{m^2 \cdot nm}\right]. \tag{2}$$

In Fig. 1 hatching shows the range of temperatures and wavelengths of radiation in which the difference between formulas (1) and (2) is less than 1% - the Wien's region. Thus, for =500 nm, the Wine approximation is correct up to temperatures $T < 6000$ K, for =1.5 μm - up to $T < 2000$ K. The same figure exemplifies the black
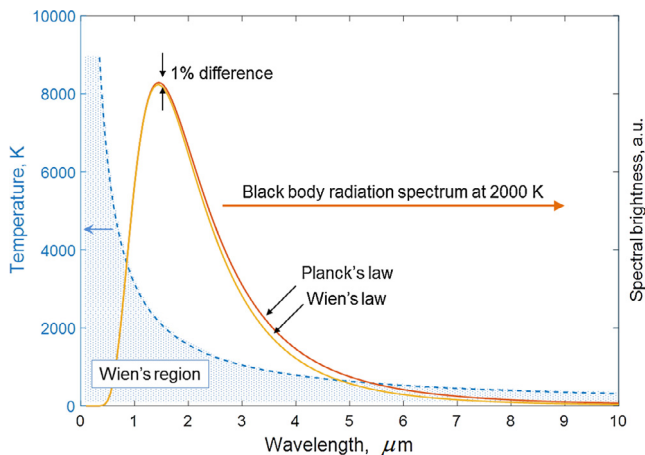

Fig. 1. The Wien's region in the coordinates «radiation wavelength – source temperature» and black body radiation spectrum at 2000 K.

body thermal radiation spectrum at 2000 K calculated by the Plank's (1) and Wien's (2) formulas. The Wien's region features the exponential dependence of the spectral brightness of the radiation on the temperature, which provides high sensitivity of measuring instruments and allows to reach high measurements accuracy (error below 0.1%). Further analysis of the pyrometry methods is presented by the authors for this very region.

Individual features of the atomic and crystalline structure of materials, which determine the availability of energy electronic levels, lead to the fact that the spectrum of thermal radiation of real bodies $b(\lambda,T)$ differs from the spectrum of the black body $r(\lambda,T)$. The dimensionless value of the material spectral emissivity $0 \leqslant \varepsilon(\lambda,T) \leqslant 1$ is defined by the relation

$$\varepsilon(\lambda,T) = b(\lambda,T)/r(\lambda,T). \tag{3}$$

The emissivity is the radiation property of a material. In the general case, it depends on the radiation wavelength, body temperature, its surface condition, observation angle and other properties. For most metals in the optical wavelength range (400–800 nm), the normal emissivity decreases with increasing wavelength and increases with increasing temperature, and its typical values lie in the range 0.3–0.5 [5]. Those bodies which emissivity does not depend on the wavelength are referred to as «grey bodies». For example, coal is a grey body in a wide range of wavelengths with a value of $\varepsilon = 0.8-0.9$ [6]. Calibration and verification of pyrometric instruments use reference radiation sources– black body models providing values $\varepsilon \approx 0.99$, as well as temperature lamps with a tungsten ribbon, for which the emissivity properties are well studied [5,7].

3. Review of up-to-date pyrometry methods

Having the formulas (1) or (2) available, it is possible to determine the temperature of the black body by measuring the intensity of its radiation in one or several wavelength ranges. The determination of the temperature of real objects is complicated by the fact that their radiation can significantly differ from Planck's law due to an arbitrary dependence $\varepsilon(\lambda)$. For this reason, all the pyrometric methods operate with conventional (observed) temperatures, for the determination of which the results of observations of the real object are compared to intensity of the radiation of the blackbody.

3.1. Brightness pyrometry

In the brightness pyrometry method (also called single color pyrometry), the intensity of the monochromatic radiation of an object at a selected wavelength $b(\lambda_0)$ is measured. The *brightness temperature* T_{br} of an object is the temperature at which the black body has the same spectral brightness at the selected wavelength λ_0 as the body under consideration at the true temperature T:

$$b(\lambda_0,T) = r(\lambda_0,T_{br}). \tag{4}$$

Using the formulas (2)–(4), one can easily define the relation between the brightness and true temperatures of the studied body:

$$\frac{1}{T_{br}} = \frac{1}{T} - \frac{\lambda_0}{C_2} \ln \varepsilon(\lambda_0, T). \tag{5}$$

Evident that the brightness temperature of the body (the observed one) is always lower than its true temperature due to the inequality $0 \leqslant \varepsilon \leqslant 1$. For example, for tungsten at 2000 K, the brightness temperature is 1860 K ($\lambda_0 = 650$ nm, $\varepsilon = 0.43$), i.e. 7% lower. Large methodical errors of the temperature measurement are the major disadvantage of the brightness pyrometry. It is should be noted that the brightness pyrometers require re-calibration, i.e. establishment of the correspondence between the measured signal level and the object brightness temperature $b \leftrightarrow T_{br}$ at any variation of the instrument optical channel (lens focal distance, aperture value, observation distance, etc.). However, it is precisely the brightness pyrometers that have received extremely wide practical applications because of their simplicity: the installation of a narrow-band filter and calibration with a temperature standard turn a suitable photodetector into a brightness pyrometer. The cameras based on 2D CCD- and CMOS-arrays allow to register the spatial distribution of the temperature over the surface of nonuniformly heated bodies and particle ensembles [8,9], whereas photomultipliers and photo-diodes of various types allow to perform local measurements with the frequency up to 4 GHz [10] and over.

3.2. (Two-) color pyrometry

The two-color pyrometry, or the spectral ratio method, is based on measuring the intensity of the radiation of an object at two wavelengths λ_1 and λ_2. The color temperature T_c of the object is the temperature at which the ratio of the spectral brightness of the blackbody $r(\lambda, T_c)$ at selected wavelengths λ_1 and λ_2 is the same as in the radiation of the observed object at the true temperature T:

$$\frac{b(\lambda_1, T)}{b(\lambda_2, T)} = \frac{r(\lambda_1, T_c)}{r(\lambda_2, T_c)}. \tag{6}$$

The relation between the observed color temperature and true body temperature is found from the definition (6) involving (2) and (4):

$$\frac{1}{T_c} = \frac{1}{T} + \frac{\lambda_1 \lambda_2}{C_2} \frac{\ln(\varepsilon_1/\varepsilon_2)}{(\lambda_1 - \lambda_2)}, \tag{7}$$

where ε_1 and ε_2 are the emissivities of the body at the wavelengths λ_1 and λ_2, respectively. The color temperature equals to the true body temperature for the grey objects with $\varepsilon_1 = \varepsilon_2$. In the above example of tungsten at 2000 K, the color temperature measured at a pair of wavelengths of 640 and 660 nm is 2044 K, that is, the methodical error is only 2%. Usually, the difference between T and T_c is less than between T and T_{br}, therefore the latter method is more preferable when the objects with an unknown emissivity are investigated. Moreover, the readings of color pyrometers are not sensitive to varying observation conditions at which the signal level changes proportionally in both channels – variation of the distance to the object, partial image covering, etc. Simplest two-color pyrometers can be based on color video cameras [11]. There is a widespread misconception [12–14] that the choice of wavelengths λ_1 and λ_2 sufficiently close allows to avoid the influence of an unknown object emissivity, since it could be considered $\varepsilon_1 \approx \varepsilon_2$ and $\ln(\varepsilon_1/\varepsilon_2) \to 0$. But in this case, the denominator $(\lambda_1 - \lambda_2)$ also trends to zero, and the value of derivative $d(\ln \varepsilon)/d\lambda$ is important.

It is noteworthy that the brightness pyrometers possess the higher temperature sensitivity (resolution) than the two-color ones. The reason is that in the brightness method, the measured signal is the spectral brightness of the objects on the chosen wavelength $s = b(\lambda_0)$, whereas in the two-color pyrometers, it is the brightness ratio in two wavelengths $s = b(\lambda_1)/b(\lambda_2)$. Fig. 2 shows the signal range the brightness and two-color pyrometers under observation of the black body. As the body temperature varies from 2000 to 3000 K, the signal of the brightness pyrometer increases 100 times, the one of the two-color pyrometer increases only 1.6–5 times, depending on the chosen operation wavelengths. For example, when measuring the object temperature at about 2000 K, with the instrumental error of direct measurements of 1%, the random error of the brightness pyrometer is 1.5 K (0.075%), the one of the two-color pyrometer is 7–30 K (0.35–1.5%).

3.3. Multi-wave pyrometry

To improve the accuracy of temperature measurements, multi-wave methods are used, based on registration the thermal radiation of an object in several spectral ranges and repeatedly applying a brightness or color approach to different wavelengths or wavelength pairs. For example, the objects radiation brightness $b(\lambda_i)$ is registered at several wavelengths λ_i, $i = 1, 2, 3 \ldots n$, and its temperature is found by the curve fitting method, minimizing the residual to the grey body radiation spectrum [15]:

$$\phi = \sum_{i=1}^{n} (b(\lambda_i) - \varepsilon \cdot r(\lambda_i, T))^2 \to \min. \tag{8}$$

If there is *a priori* information on the spectral dependence of the material emissivity, its use can further reduce the methodical error of measurements [16]. Another approach is the multiple calculation of the object's color temperature using different wavelength pairs λ_i, λ_j, which allows obtaining a statistical set of values $T_{i,j}$ [17]. In this case, the most probable value from the obtained distribution is considered to be the measured temperature.

The considered multi-wave methods do not allow to formalize the relationship between the measured and true temperature of the object. In addition, they are local, i.e. do not register the spatial distribution of temperature.

3.4. Spectral pyrometry

The development of semiconductor microelectronics over the past 15 years has significantly increased the availability of photo-spectrometers based on linear CCD and CMOS arrays. Such devices allow registration of radiation over a wide range of wavelengths, for example, several thousand values in the spectral range 0.2–1.1 μm (Si) or 0.9–2.5 μm (InGaAs). For this reason, the method of spectral pyrometry has received wide application, a detailed review of which is presented in [18]. Large number of discrete measurements $b(\lambda_i)$ $i = 1, 2, 3 \ldots n$ provides a series of advantages. First, the random (instrumental) error of temperature measurements is significantly reduced in comparison with the two-color method (the dependence $1/\sqrt{n}$), and secondly, it is possible to verify directly during the experiment that the observed emission spectrum is purely thermal, without an exterior component (lines or bands of excited atoms and molecules, chemo-luminescence, etc.). In addition, from the methodical point of view it is important that it becomes possible to restore the continuous thermal spectrum of the object $b(\lambda)$ and to calculate its derivative.

The temperature measurement from the registered continuous spectrum can be done by the considered multi-wave methods, however in the Wien's region, it is convenient to use auxiliary variables:

$$x = C_2/\lambda, \quad y = \ln(r\lambda^5), \tag{9}$$

in which the black body radiation spectrum (2) takes the linear form: $y = -x/T + const$, and its temperature is found from the plot slope angle: $T = -(dy/dx)^{-1}$. Similarly to the above mentioned definitions of the brightness and two-color temperature of the real
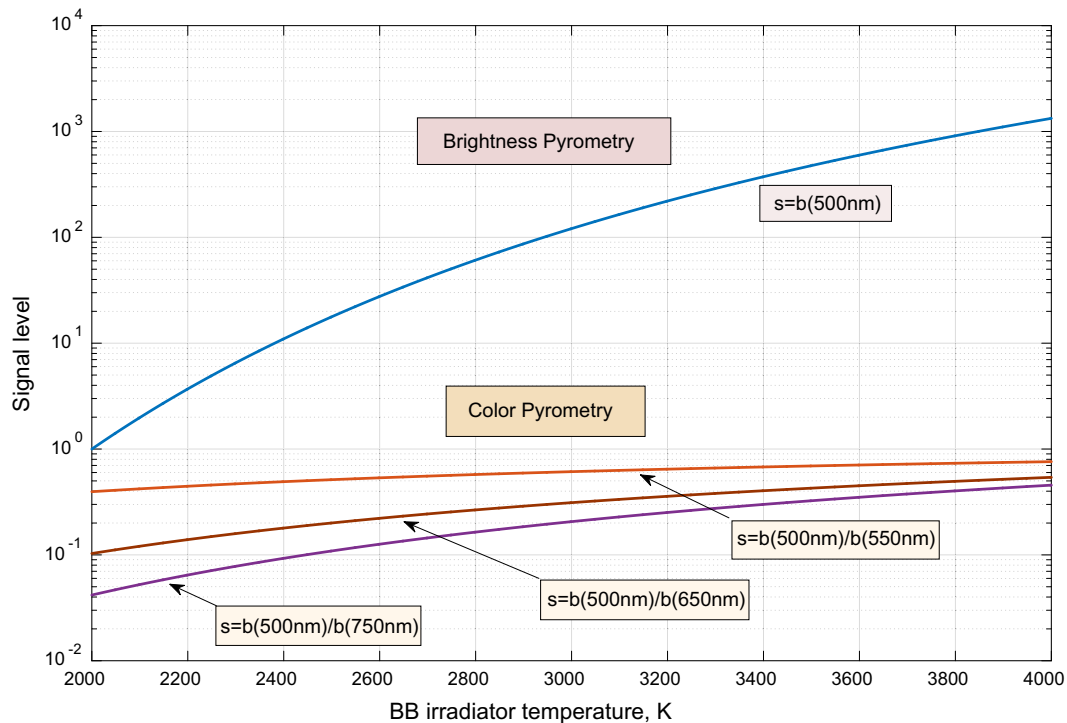
Fig. 2. Dependence of the measured signal in the brightness and two-color pyrometry methods on the black body temperature in the range 2000–4000 K. The brightness pyrometer signal ($\lambda_0 = 500$ nm) is rated to the signal level at T = 2000 K. The signal of the two-color pyrometer is given for three wavelength pairs λ_1 / λ_2: 500/550 nm, 500/650 nm, 500/750 nm. (For interpretation of the references to colour in this figure legend, the reader is referred to the web version of this article.)

body, let us introduce the definition of the *spectral temperature*: the temperature T_s, at which the black body radiation spectrum has the same derivative dy/dx in the chosen point $x = C_2/\lambda$, as the spectrum $\ln(b\lambda^5)$ of real radiating object at the true temperature T:

$$\left. \frac{d\ln(b\lambda^5)}{dx} \right|_T = \left. \frac{dy}{dx} \right|_{Ts}. \qquad (10)$$

With such a definition, it is easy to establish the relation between the observed spectral temperature T_s, measured in the vicinity of wavelength λ, and the true object temperature T:

$$\frac{1}{T_s} = \frac{1}{T} + \frac{\lambda^2}{C_2} \frac{d\ln\varepsilon}{d\lambda}. \qquad (11)$$

It is clear from the formulas (10) and (11) that the measured value of the spectral temperature T_s coincides with the true temperature T for the grey body. In the review [18], it is noted that it is spectral pyrometry that makes it possible to measure the true values of the temperature of objects with an unknown emissivity when operating in the short-wave spectral region due to a relatively fast (proportional to λ^2) decrease of the second term on the right-hand side of formula (11). However, as can be seen from formulas (7) and (5), the same applies to the method of color pyrometry and, to a lesser extent, to the brightness method. In practice, the most important advantage of spectral pyrometry is the possibility of selecting the operating wavelength and transferring measurements to the short-wave region without changing the instrument hardware (replacing the bandpass filters or readjusting monochromator) and repeating the measurements.

In addition, the instrumental (random) error of spectral temperature measurements decreases as $n^{-1/2}$, where n – the number of registered wavelengths. For example, if we return to example with an object at temperature 2000 K, and inaccuracy of direct measurements of 1%, the instrumental error of spectral pyrometer having

400 operating wavelengths would be 0.5–1.5 K (0.025–0.075%) which is better than that of the brightness pyrometer.

Comparison of the formulas (7) and (11) shows that the two-color pyrometry is the discrete analog of the spectral method, in which the derivatives are preplaced by finite differences. That is why the methodical error of the temperature measurement related to the unknown emissivity of the material, is the same for the two-color and spectral pyrometry methods when operating in the same spectral ranges.

In recent years, the hyper-spectral cameras have become available; they form images either via scanning the elements of the object surface, or via registering a series of monochromatic images during the re-adjustment of acousto-optic or liquid-crystal band filter [19,20]. It results in a long duration of the measurements (registration of the hyper-spectral image, size 1024 × 1024 at the spectral depth of 500 wavelengths and exposure 1 ms takes about 1 s), which makes it inapplicable for the fast process diagnostics.

The low level of the registered signal (the radiation is distributed between thousands of registering elements) is the flip side of the registration of a wide range of the radiation spectrum, thus normally spectral instruments have long exposure time, or a larger size of observation area compared to the brightness instruments. For this reason, the question arises as what temperature is measured by the spectral pyrometer in the case of considerable temperature variations during the signal registration or at the non-uniform temperature distribution in the observation region? In [21] it is correctly noted that this measured spectral temperature «is close to maximum», but this estimation has no quantification. Earlier, there were attempts to restore the temperature distribution in the observation region by the registered total spectrum [22,23], but this approach turned out to be extremely unstable. For example, it was demonstrated in [24] that when there is a comparatively weak noise in the registered spectrum (450–850 nm) at a level 0.1–0.3%, there is a significant distortion of the restored tempera-

ture distribution of 1000–3000 K up to the physically incorrect shape. Similar results were obtained in [25] for the spectral range of 8–13 μm and temperature range 500–800 K.

4. Spectral-brightness pyrometry

The given brief review shows two basic approaches to the pyrometric measurements of the temperature – by the absolute intensity (the brightness one), and by the shape of the thermal radiation spectrum (the spectral, two-color one). The former one features the high spatial and temporal resolution of the measurements, has high sensitivity to weak temperature variations, but requires the absolute calibration and demonstrates high methodical errors for the materials with the low emissivity. The latter does not require the absolute calibration, measures the true temperature in the case of grey bodies, but is local and relatively slow. In this work we propose the pyrometric method combining the potentials of two above discussed approaches, the spectral-brightness pyrometry method (SBP).

The essence of the SBP method is that when observing the object with the unknown emissivity and non-uniform temperature distribution over the surface (and/or over the time), two registration channels with common field of view (FOV) are used: the spectral channel registers the total (integral) thermal radiation spectrum from FOV, whereas the brightness one – the spatial (and/or the temporal) distribution of brightness at the chosen wavelength in FOV. As a result it is possible to restore the temperature distribution in the FOV, having the methodical accuracy of the spectral method, and sensitivity and spatial (and/or temporal) resolution of the brightness method.

To be definite, let us consider the photo-detecting array registering the spatial distribution of the thermal radiation intensity from the object surface as the brightness channel; the surface elements have the temperature T_i, where $i = 1, 2, 3 \ldots n$. The operational wavelength of the brightness channel λ_o is chosen such that the Wien's formula (2) remains valid within the considered temperature range. The emissivity of the material is unknown but is considered to be constant $\varepsilon(\lambda, T) = const$ within the range of the measured temperatures in the spectrum region near λ_o. According to the formulas (2) and (3), the temperature T_i of the object surface individual element is related with the level of the signal of the photo-array element as follows:

$$b_i = A \cdot \varepsilon \cdot r(\lambda_0, T_i) \cdot ds \cdot dt = A_1 \cdot \exp\left(-\frac{x_o}{T_i}\right), \tag{12}$$

where $A_1 = const$ is the camera sensitivity at the fixed parameters of its optoelectronic channel (optical magnification, lens aperture, exposure time, etc.), ds is the individual surface element area, dt is the photo-detector exposure time, $x_o = C_2/\lambda_o$. The area of the surface elements ds, as well as the exposure time dt should be chosen such that the temperature of each element T_i could be considered constant during the observation. According to the formula (12), arbitrary levels of the signal b_i, b_o of the digital camera are related with respective surface elements temperatures T_i and T_o by the expression

$$\frac{1}{T_i} = \frac{1}{T_o} + \frac{\lambda_o}{C_2} \ln \frac{b_o}{b_i}. \tag{13}$$

The spectral channel registers the spectrum of the total thermal radiation from the same object area as the brightness channel. The spectrometer signal, according to the formulas (2) and (3), equals to:

$$S(\lambda) = B \cdot \varepsilon \cdot ds \cdot dt \cdot \sum_i r(\lambda, T_i) = \frac{B_1}{\lambda^5} \sum_i \exp\left(-\frac{C_2}{\lambda T_i}\right), \tag{14}$$

where $B_1 = const$ is the spectrometer sensitivity involving all properties of its optical channel. After conversion to Wien's coordinates $x = C_2/\lambda$ and $y = \ln(S\lambda^5)$, the relation (14) takes form:

$$y(x) = \ln(B_1) + \ln\left(\sum_i \exp(-x/T_i)\right). \tag{15}$$

In accordance with the spectral pyrometry method, let us define the reference temperature T_o as the temperature of the grey body which thermal radiation spectrum has the same derivative value in the point x_o, as the integral spectrum (14):

$$T_o(x_o) = -(dy/dx)^{-1}|_{x=x_o}. \tag{16}$$

Let us calculate the reference temperature T_o in the range of the registered spectrum near x_o. Here, T_o may not belong to the set of the individual temperatures T_i of object surface elements, which really exist in the observation region. On the other hand, T_o can be expressed through the set of T_i from the formula (15) in accordance with (16):

$$\frac{1}{T_o} = \frac{\sum_i \frac{1}{T_i} \cdot \exp(-x_o/T_i)}{\sum_i \exp(-x_o/T_i)}. \tag{17}$$

Expressing the set of temperatures T_i in (17) using the formula (12) through the signal levels b_i of the image elements registered by the digital camera, we have:

$$\frac{1}{T_o} = \frac{1}{x_0}\left(\ln A_1 - \frac{\sum_i b_i \cdot \ln b_i}{\sum_i b_i}\right) \quad \text{or} \quad \exp\left(\frac{\sum_i b_i \cdot \ln b_i}{\sum_i b_i}\right)$$
$$= A_1 \exp\left(-\frac{T_o}{x_0}\right). \tag{18}$$

Comparison of (12) and (18) demonstrates that we obtained the definition formula of the reference signal level b_o, corresponding to the reference temperature T_o:

$$b_o = \exp\left(\frac{\sum_i b_i \cdot \ln b_i}{\sum_i b_i}\right). \tag{19}$$

After this, it is easy to determine the set of temperatures T_i of all surface elements by formula (13). Thus, utilization of the spectral channel to register the radiation in the SBP method enables to perform the thermal vision camera calibration (to establish the correspondence $b \leftrightarrow T$) directly during the object investigation. Note that the true object temperature, not the brightness temperature, is found for the grey object.

Evident that in the case of a grey body the unknown value of the object emissivity ε does not affect the measurement results. In particular, no additional measurement errors arise during investigation of surfaces with low emissivity $\varepsilon < 0.1$ [26].

As for the case of «non-grey» bodies, the complete analysis of temperature measurement errors in SBP method is quite difficult as it should take into account arbitrary dependence of emissivity $\varepsilon(\lambda, T)$ and deserves an individual research. Nevertheless let us indicate the main methodical errors of SBP. In the case of material emissivity having solely spectral dependence $\varepsilon(\lambda)$, but no temperature dependence, the error of measuring reference temperature T_0 is described by the formula (11) and is the same as in spectral and two-color methods. This methodical error in calculation of T_0 value will spread to calculation of individual surface elements temperatures T_i using Eq. (13), e.g. 2% error for tungsten at 2000 K. The brightness channel of SBP pyrometer system is not effected by

dependence $\varepsilon(\lambda)$, because it operates only at selected wavelength λ_o.

The effect of temperature dependence of object emissivity on measurements error is somewhat more difficult to formalize basing on formula (11), but one can see that for real materials this effect isn't critical because dependence $\varepsilon(T)$ is usually weak compared to $r(\lambda_0, T)$. For example, when tungsten surface temperature increases from 2000 to 2200 K its emissivity reduces only by 1%, while its spectral brightness (λ_0 = 500 nm) rises 5 times. Therefore approximation $\varepsilon(T_i) \cdot r(\lambda_0, T_i) \approx \varepsilon \cdot r(\lambda_0, T_i)$ remains valid for real objects in typical temperature ranges available for registration by optical instruments. For the same reason calculation of individual surface elements temperatures T_i using formula (13) remains practically unaffected by weak dependence $\varepsilon(T)$ owing to valid approximation $\varepsilon(T_0)b_0/\varepsilon(T_i)b_i \approx b_0/b_i$.

It is important to note that the SBP allows to determine not only the spatial distribution of temperature, but also its temporal dynamics. In the case of local temperature measurement $T(t)$, i.e. when the FOV is a single point, the brightness channel registers the local dynamics of brightness $b_i = b(t_i)$, whereas the spectral channel registers the integral radiation spectrum accumulated during the total observation time. Similarly, in the case of measurement of the temperature field dynamics $T(t,x,y)$ in a certain region S, the brightness channel registers the spatial and temporal distribution of the thermal radiation brightness $b_i = b(t_i,x_i,y_i)$, where $(x_i, y_i) \in S$, and the spectral channel registers the spectrum of the total radiation from the region S during the total observation time. In every considered case, the resulting formulas (15)–(18) do not change their form. The only condition for application the SBP method is that the initial assumptions of the method are satisfied: the material emissivity is constant, and every individual surface element ds has invariable temperature during exposure time dt of the brightness channel.

5. Examples of SBP implementation

5.1. Temperature field measurements

Let us demonstrate some examples of the practical application of the SBP method. Fig. 3 shows the experimental setup used by the authors to determine the non-uniformity of the temperature distribution on the tungsten band of the temperature lamp TRU-1100-2300. The lamp is the calibration source of the thermal radiation within the temperature range of 1100–2300 K, its certificate of verification contains a correspondence table «band temperature – lamp current» with an accuracy of 10 mA. The uncertainty of

current stabilization for the used power source PSW7 30–36 (GW Instek, Taiwan) is 40–50 mA, which leads to the temperature reproduction accuracy of 4–8 K. However, the real temperature deviations on the band surface may essentially exceed this value due to non-uniform band heating.

The thermal radiation of the band surface was registered using the digital camera HD1-1312-80-G2 (Photonfocus AG, Switzerland), with a narrow-band filter installed in the optical channel: CWL 575 nm, FWHM 50 nm. The spatial resolution of recording was 40 μm /pixels. LR1-T (Aseq Instr., Canada) photospectrometer with sensitivity range 300–1000 nm and nominal spectral resolution 0.2 nm was used for registration of the integral spectrum. Spectrometer FOV had the diameter of 10 mm and was located in the center of the camera frame (marked with the dashed circle in Fig. 3b, and 4b–e).

The integral radiation spectrum, as well as the spatial distribution of brightness $b(x,y)$ over the tungsten band surface were registered for each of four values of the lamp current I = 10, 15, 20, 25 A. Fig. 4, a shows four integral radiation spectra of the tungsten, the red marker points the operational wavelength of the brightness channel λ_o = 575 nm. The reference temperature T_o was calculated from the 40 nm wide spectral region (200 wavelengths). The insertion shows the same spectra in the Wien's coordinates, plus the tangent line to the plot in the point $x_0 = C_2/\lambda_o = 25,023$ K, which was used to calculate spectral temperature T_o by the formula (16). The signal-to-noise ratio (SNR) of registered spectra for filament currents I = 10, 15, 20, 25 A equal to $9.5 \cdot 10^3$, $9.1 \cdot 10^4$, $2.4 \cdot 10^6$, $2.6 \cdot 10^4$, respectively, which provided instrumental (random) error of reference (spectral) temperature calculation $dT_0 = 9{-}16$ K just little higher than accuracy of the power source.

On the base of the formula (19), the reference brightness b_o was found for the area inside spectrometer field of view; then the temperature field $T(x,y)$ was calculated using the formula (13). Importantly, after determining the values of T_o and b_o, it is possible to calculate the temperatures of surface elements even outside the spectrometer FOV. In fact, the SBP allows automatic calibration of the brightness pyrometer which remains valid provided the material's emissivity is unchanged.

Fig. 4b presents the temperature distributions on the tungsten band surface obtained at the lamp currents of 10, 15, 20, 25 A which allow us to study in detail the non-uniformity of its heating. Contour lines on the presented temperature maps correspond to the temperature step of 10 K. Table 1 gives the results of measurement of the reference (spectral) temperature T_0, and the maximum T_{max} and average T_{av} temperatures in the spectrometer FOV. Evident that the temperature T_0 measured by the spectral method, is truly close to the maximum one T_{max}, but does not equal to it.
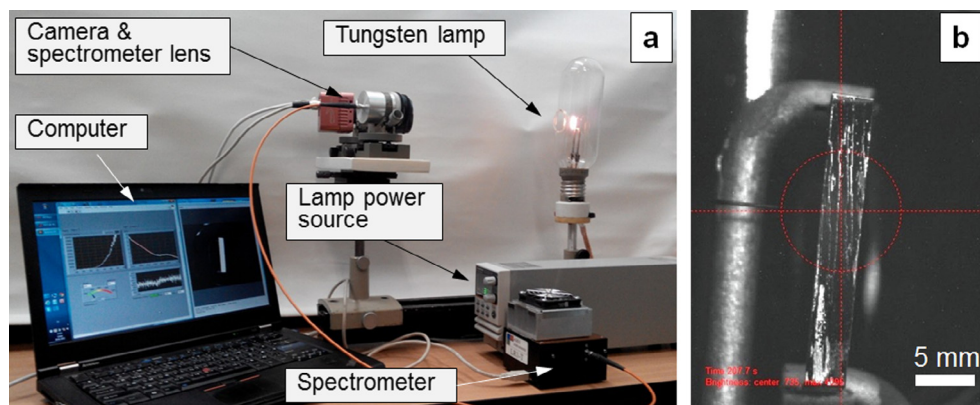

Fig. 3. Experimental setup used for investigation of the temperature distribution on the surface of tungsten band of the temperature lamp: a – external appearence, b – field of view of the digital camera and photospectometer.
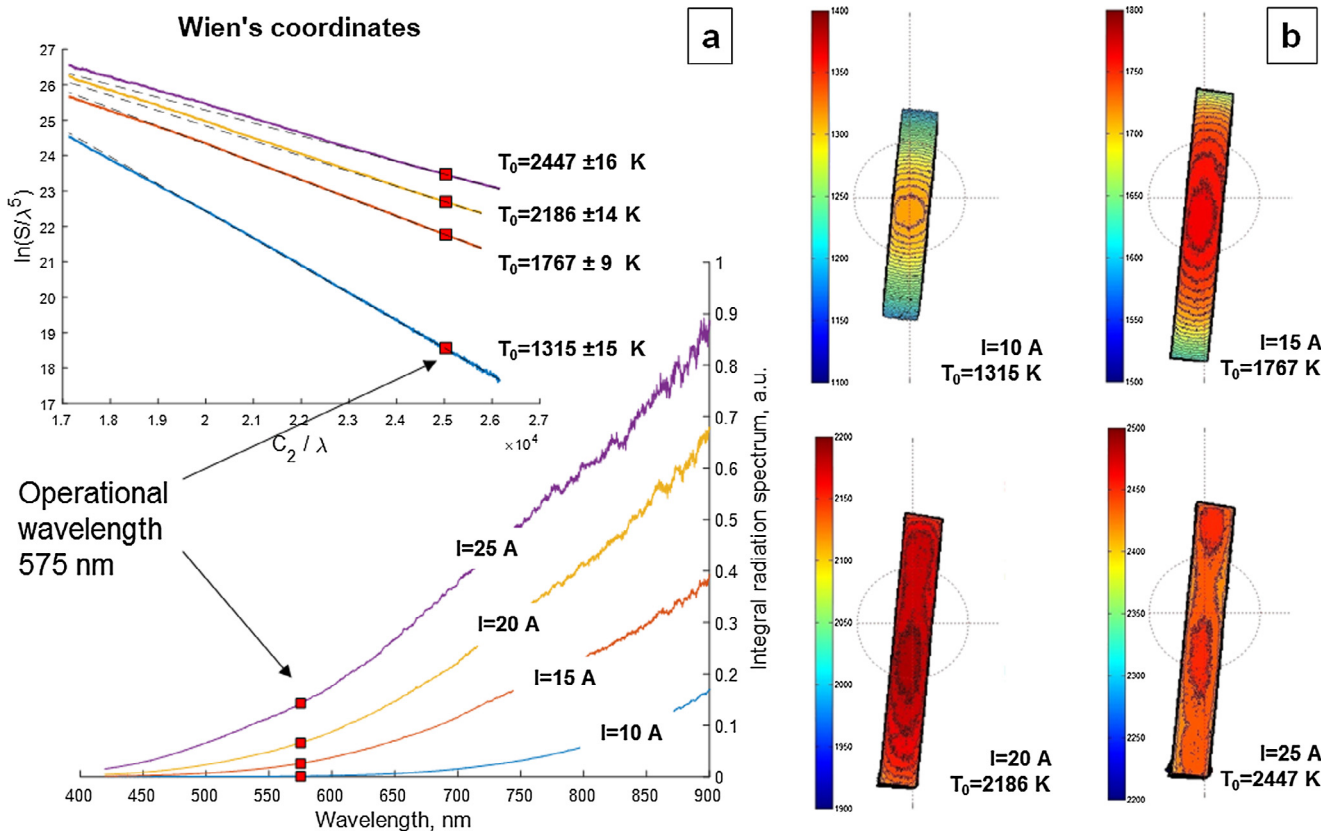
Fig. 4. Results of SBP measurements of the spatial temperature distribution over the surface of the tungsten band at the lamp currents 10–25 A: a – integral radiation spectrum; b – maps of the temperature distribution over the band surface. The values of the reference temperature are given for each spectrum in the form $T_0 \pm dT_0$. Registered spectra for different heating currents were obtained using different exposure times.

The average temperature in the spectrometer FOV may differ essentially from the measured spectral temperature, and it is the SBP method that allows to determine its value.

As is evident from Fig. 4, at the low lamp currents, the temperature distribution is essentially nonuniform on the band surface. Table 1 presents the values of the temperature spread ΔT_{4mm} in the region of 4 mm (equals to the band width). As is seen, the temperature spread may reach almost 40 K (3%) even in such a relatively small spot, which exceeds the discussed instrumental and methodical errors of the spectral pyrometry in the case of tungsten. As the current rises to 20–25 A (above 2000 K), the temperature
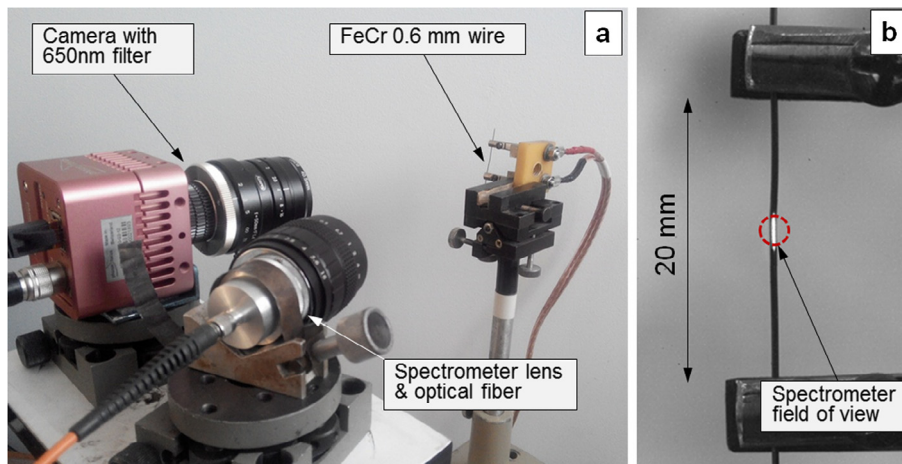
Table 1
Properties of measured temperature distribution on the surface of the tungsten lamp TRU 1100-2300.

Filament current, A	10	15	20	25
T_0/K	1315	1767	2186	2447
T_{max}/K	1321	1771	2193	2451
T_{av}/K	1282	1752	2175	2442
ΔT_{4mm}/K	38	12	7	5

Fig. 5. Experimental setup used for investigation of temperature dynamics of FeCr wire: a – external appearance, b – field of view of the digital camera and photospectometer.

spread ΔT_{4mm} approaches to 5–7 K, which roughly corresponds to the accuracy of the temperature reproduction with this power source. Thus, to increase the accuracy of the temperature measurements, the works with the reference tungsten lamps of this type should be carried out at high heating currents (band temperatures).

5.2. Temperature dynamics measurements

Let us consider the example of SBP application for investigation of the local temperature dynamics in rapid processes. Fig. 5 presents the experiment configuration used to study the heating dynamics of the FeCr wire (alloy Kh23Yu5T: Fe - balance, Cr 23%, Al 5%, Si 0.6%, Mn 0.3%) with diameter 0.6 mm, under the electric current (applied voltage 20 V). In this experiment, the same digital camera and photo-spectrometer were used, but the camera was operated at the frame rate of 1000 fps (the field of 650×100 pixels, exposure time 50 μs), whereas the photo-spectrometer registered a single spectrum with the exposure time of 1 s. The digital camera was started simultaneously with the power source, the start of the spectrometer registration was synchronized with the registration of the first video frame (hardware synchronization using the TTL signal). The operational wavelength of 650 nm was chosen for the brightness channel (the bandpass filter with CWL = 650 nm, FWHM = 50 nm). The diameter of the spectrometer FOV spot was 2 mm.

Fig. 6, a shows the integral radiation spectrum of the wire, registered by the spectrometer (the operational wavelength λ_o = 650 nm is marked in red). The calculated over 40 nm wide spectral range (200 points) reference temperature is T_0 = 1849 K.
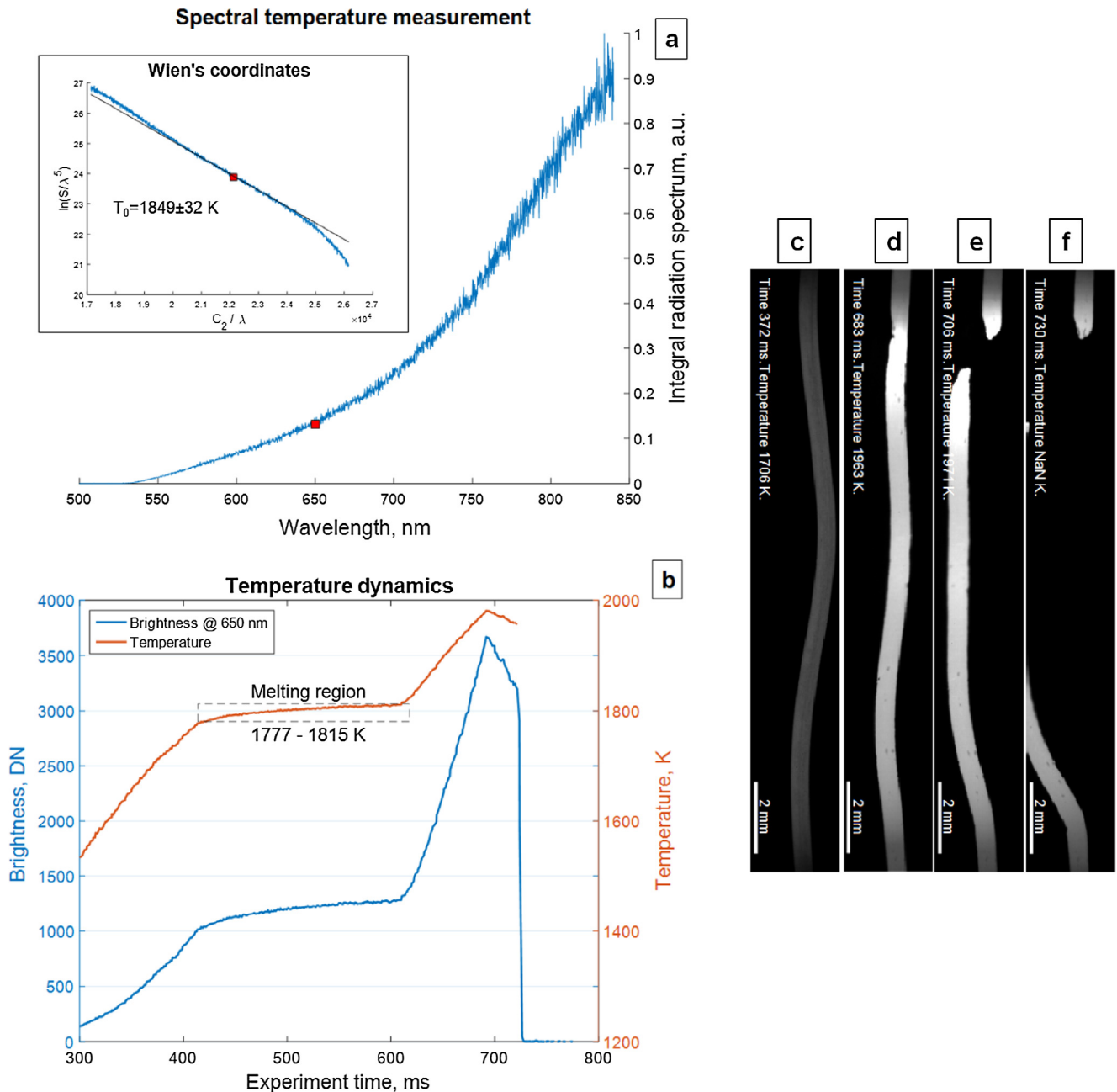

Fig. 6. Results of SBP control for the control of the dynamics of FeCr wire heating: a – integral radiation spectrum of the wire within 0–1000 ms; b – dynamics of material brightness and temperature in the spectrometer field of view; c–f – brightness images of the wire in different time moments.

Evident that the spectrum plotted in the Wien's coordinates, has the noticeable deviation from linear shape, which is related to the considerable variation of the object temperature during the measurement. Moreover, due to the long spectrometer exposure time the signal has relatively high noise level (SNR = $1.1 \cdot 10^3$), which leads to instrumental inaccuracy of reference temperature measurement $dT_0 = 32$ K. Fig. 6b shows the registered dynamics of the wire brightness b_i in the spectrometer field of view (plotted in the camera digital numbers, DN), plus the temperature T_i dynamics calculated using the formula (13). Here, index i means the correspondence to the moment of time t_i, and $t = 0$ matches the power up moment of the power source. Here we can discuss contribution of brightness channel (camera) into temperature measurement inaccuracy. The noise level of the camera CMOS-array was measured to be 15 digital numbers (DN). This instrumental inaccuracy corresponds to temperature error 1–3 K (in signal range 500–3500 DN), which is an order of magnitude lower than spectral channel uncertainty.

The plot of wire temperature dynamics shows an extended plateau at the level of 1777–1815 K within the time period of 410–620 ms. This interval obviously corresponds to the material melting process, whereas the rated melting point of Kh23Yu5 T alloy is 1773 K (1500 °C). It should be stressed that the overall error of the experimental temperature measurement appeared to be just 0.2–2.4% without involvement of any information on the material emissivity. Furthermore, this error is obtained under conditions where the material emissivity could change during its phase transition (melting).

The material temperature in Fig. 6 continues to rise to the maximum value of 1951 K and stops at $t = 690$ ms because of the rupture of the melted wire and breakdown of the electric current. At $t = 720$ ms, the wire bends and goes out of pyrometer FOV. The data from Fig. 6 allow one to calculate that the material heating rate before the melting ($t = 300$–400 ms) and after it ($t = 620$–690 ms) is similar and equals to $2.1 \cdot 10^3$ K/s. On the other hand, the metal cooling rate at $t = 690$–720 ms is about three times lower and makes $0.78 \cdot 10^3$ K/s. Fig. 6c–f presents the brightness images of the wire at different moments of time: before melting (372 ms), after melting and right prior to the breakdown (683 ms), right after the breaking (706 ms), and during the wire bending (730 ms). Interestingly, the measured wire temperature in the bending elbow (Fig. 6d–f) is 1790–1810 K, i.e. also corresponds to the material melting point.

The presented examples demonstrate the basic capabilities of the SBP method for the analysis of the spatial temperature distribution $T(x, y)$ on the object surface, as well as the dynamics of the local temperature $T(t)$ variation. Quite evident that this approach can be directly used to study the dynamics of the temperature field $T(t, x, y)$ variation. Special adaptation of the method allows diagnostics of moving dispersed particles of the material (sizes 20–100 μm, speed 100–700 m/s) in thermal spraying processes [27–29]. In the general case, the SBP is advantageous for diagnostics of fast high-temperature processes in which present spectral instruments are not able to provide the required time performance and spatial resolution.

6. Conclusions

Presented analysis of modern pyrometric methods shows that there are two basic approaches to the radiometric temperature measurement: by the absolute intensity of the thermal radiation, the brightness one, and by the spectrum shape, the spectral one. The brightness pyrometry method permits performing the temperature measurements with high sensitivity to the temperature, with high spatial and temporal resolution. The disadvantage of this

method is the high methodical error related with the unknown value of the material emissivity ε. In practice, the methodical error of the spectral pyrometry is much lower, since it depends on the value of derivative $d\varepsilon/d\lambda$, and disappears in the case of the grey objects providing measurements of the true temperature. Nevertheless, the present spectral instruments are not able to provide the same measurements response time and spatial resolution as the brightness pyrometers.

In this work, the authors propose and mathematically substantiate the new spectral-brightness pyrometry method, which allows to integrate the strong points of the spectral and brightness approaches. The measurements are carried out in the spectral range satisfying the Wien's approximation; the grey body thermal radiation is suggested, i.e. $\varepsilon = const$. The measurements involve the simultaneous registration of spatial and/or temporal distribution of brightness of object's thermal radiation at the operational wavelength λ_0 and integral radiation spectrum in the range including λ_0. Self-calibration of the pyrometric system is based on the comparison of the reference spectral temperature T_0, calculated using the registered spectrum, and reference brightness value b_0, which presents the weighted average brightness value over the observation region.

The presented simple examples of the SBP realization demonstrate the capabilities of the measurement of the spatial temperature distribution over the object surface (the tungsten band of the calibration lamp TRU 1100-2300, temperature 1300–2500 K, spatial resolution 40 μm), and the local temperature dynamics (heating of the FeCr wire, temperature 1500–2000 K, temporal resolution 1 microsecond). The analysis of measurement errors shows that SBP is capable of temperature measurements with 1–2% accuracy without employment of any information about material emissivity properties. The SBP is advantageous for diagnostics of fast high-temperature processes in which present spectral instruments are not able to provide the required time performance and spatial resolution, and the applicability of the brightness methods is limited by the unknown or varying material emissivity.

Acknowledgements

References

[1] Traité de pyrométrie optique: Encyclopédie photométrique/Ed. by G.Ribaud. – Paris: Revue d'Optique, 1931.

[2] Temperature measurements. L. Michalski, K. Eckersdorf, J. Kucharski, J. McGhee. – second ed., Chichester: John Wiley & Sons, 2001, 478p.

[3] Optical methods of real temperatures measurements. D.Ya. Svet.– Moscow: Nauka, 1982, 296p.

[4] Radiometric temperature measurements. I. Fundamentals/Ed. by Z.M. Zhang, B.K. Tsai, G. Mashin. Experimental Methods in the Physical Sciences. V.42. – Amsterdam: Elsevier, 2010.

[5] Emissive properties of solid materials. A reference book/ Edited by: A.E. Shejndlin – Moscow, Energija, 1974, 472p. (In Russian).

[6] Physical Magnitudes: A reference book/Ed. by: I.S. Grigor'ev, E.Z. Mejlikhov – Moscow: Energoatomizdat, 1991, 1232p. (in Russian).

[7] Measurements of the optical radiation in electronics. Epshtein M.I. – Moscow: Energoatomizdat, 1990, 254 p. (In Russian).

[8] Y.-C. Lin, A.S. Shteinberg, P.J. McGinn, A.S. Mukasyan, Kinetics study in TieFe$_2$O$_3$ system by electro-thermal explosion method, Int. J. Therm. Sci. (2014) 84, article 369e378.

[9] I. Smurov, M. Doubenskaia, S. Grigoriev, A. Nazarov, Optical monitoring in laser cladding of Ti$_6$Al$_4$V, J. Therm. Spray Technol. 21 (6) (2012) 1357–1362.

[10] P.A. Ni, F.M. Bieniosek, W.L. Waldron, Multichannel optical pyrometer for sub-nanosecond temperature measurements at NDCX-I/II, High Temp.-High Press. 40 (2) (2011) 151–160.

[11] H. Guo, J.A. Castillo, P.B. Sunderland, Digital camera measurements of soot temperature and soot volume fraction in axisymmetric flames, Appl. Opt. 52 (33) (2013) 8040–8047.

[12] I. Bonefacic, P. Blecich, Two-color temperature measurement method using BPW34 PIN photodiodes, Eng. Rev. 35 (3) (2015) 259–266.

[13] A. Tapetado, J. Dıaz-Alvarez, M.H. Miguelez, C. Vazquez, Two-color pyrometer for process temperature measurement during machining, J. Lightwave Technol. 34 (4) (2016) 1380–1386.

[14] B.H. Wang, B.Q. Li, H. Yang, Y. Bai, Radiation spectral analysis and particle temperature/velocity measurement in plasma spray with one-color camera, 2017, J. Therm. Spray Technol. 20 (July 2017) 1–9.

[15] S.C. Gupta, S.G. Love, T.J. Ahrens, Shock temperature in calcite (CaCO$_3$) at 95–160 GPa, Earth Planet. Sci. Lett. 201 (1) (2002) 1–12.

[16] A.A. Mikhalchenko, V.I. Kuzmin, D.V. Sergachev, E.V. Kartaev, S.N. Ivanchik, I.S. Ivanchik, The heating and acceleration dynamics of Al$_2$O$_3$ particles in the axisymmetric heterogeneous flow emanating from a plasma torch with inter-electrode inserts, Thermophys. Aeromech. 21 (4) (2014) 515–527.

[17] V.N. Bodrov, Temperature and heat spectrum measurement using mathematical statistic apparatus, High Temp. 48 (4) (2010) 593–598.

[18] A.N. Magunov, Spectral pyrometry (Review), Instr. Exp. Tech. 52 (4) (2009) 451–472.

[19] N. Gupta, Hyperspectral imaging using acousto-optic tunable filters, SPIE 3718 (1999) 512–521.

[20] P.-H. Cu-Nguyen, A. Grewe, P. Feßer, A. Seifert, S. Sinzinger, H. Zappe, An imaging spectrometer employing tunable hyperchromatic microlensens, Light: Sci. Appl. 5 (4) (2016) e16058.

[21] A.N. Magunov, Spectral pyrometry of objects with a nonuniform temperature, technical physics, Russ. J. Appl. Phys. 55 (7) (2010) 991–995.

[22] P.Yu Gulyaev, V.I. Jordan, I.P. Gulyaev, A.A. Soloviev, Wien's criterion for a choice of parameters for reduction of particles temperature distribution from their full thermal cumulative spectrum, Russ. Phys. J. 51 (9-3) (2008) 69–76 (in Russian).

[23] P.Yu. Gulyaev, V.I. Jordan, I.P. Gulyaev, A.V. Dolmatov, et al. Method for detection of temperature distribution of condensed phase particles in two-phase plasma flow, 2010, Patent of Russian Federation RU2383873.

[24] V.I. Jordan, A.A. Soloviev, Approbation of methods and instrumental complexes for measurement of distributed parameters of velocity and temperature of particles on the two-phase flow, 2012, Bulletin of Ugra State University, vol. 25, no. 2, pp. 64–78 (in Russian).

[25] T.R. Fu, M. Duan, J. Tian, C. Shi, Inverse analysis of non-uniform temperature distributions using multispectral pyrometry, Infrared Phys. Technol. 76 (2016) 504–509.

[26] I.P. Gulyaev, V.I. Kuzmin, D.V. Sergachev, A.V. Dolmatov, Automated system for high-temperature materials tests in plasma flows, 2017, Multi-core processors, parallel programming, PLD, signal processing signals 7, pp. 183–190 (in Russian).

[27] A.V. Dolmatov, I.P. Gulyaev, V.I. Kuzmin, E.A. Lyskov, K.A. Ermakov, Analysis and optimization of gas-thermal spray process in terms of condensed phase velocity and temperature, Thermophys. Aeromech. 24 (1) (2017) 83–94.

[28] A.V. Dolmatov, I.P. Gulyaev, P.Yu. Gulyaev, V.I. Jordan, Control of dispersed-phase temperature in plasma flows by the spectral-brightness pyrometry method, IOP Conf. Series: Materials Science and Engineering, vol. 110, 2016, p. 012058.

[29] I.P. Gulyaev, A.V. Dolmatov, M.Yu. Kharlamov, P.Yu. Gulyaev, V.I. Jordan, I.V. Krivtsun, V.M. Korzhyk, O.I. Demyanov, Arc-plasma wire spraying: an optical study of process phenomenology, J. Therm. Spray Technol. 24 (8) (2015) 1566–1573.